



Pergamon

Acta mater. 49 (2001) 3433–3441



www.elsevier.com/locate/actamat

## MICROMECHANICAL AND MACROMECHANICAL EFFECTS IN GRAIN SCALE POLYCRYSTAL PLASTICITY EXPERIMENTATION AND SIMULATION

D. RAABE<sup>†</sup>, M. SACHTLEBER, Z. ZHAO, F. ROTERS and S. ZAEFFERER

Max-Planck-Institut für Eisenforschung, Abt. Mikrostrukturphysik und Umformtechnik, Max-Planck-Str. 1,  
40237 Düsseldorf, Germany

( Received 14 March 2001; received in revised form 15 June 2001; accepted 15 June 2001 )

**Abstract**—A polycrystalline aluminum sample with a quasi-2D single layer of coarse grains is plastically deformed in a channel die plane strain set-up at ambient temperature and low strain rate. The microtexture of the specimen is determined by analysis of electron back scattering patterns obtained in a scanning electron microscope. The spatial distribution of the plastic microstrains at the sample surface is determined by measurement of the 3D plastic displacement field using a photogrametric pixel-based pattern recognition algorithm. The initial microtexture is mapped onto a finite element mesh. Continuum and crystal plasticity finite element simulations are conducted using boundary conditions which approximate those of the channel die experiments. The experimental and simulation data are analyzed with respect to macromechanical and micromechanical effects on grain-scale plastic heterogeneity. The most important contributions among these are the macroscopic strain profile (friction), the kinematic hardness of the crystals (individual orientation factors), the interaction with neighbor grain, and grain boundary effects. Crystallographic analysis of the data reveals two important points. First, the macroscopic plastic strain path is not completely altered by the crystallographic texture, but modulated following soft crystals and avoiding hard crystals. Second, grain-scale mechanisms are strongly superimposed by effects arising from the macroscopic profile of strain. The identification of genuine interaction mechanisms at this scale therefore requires procedures to filter out macroscopically induced strain gradients. As an analysis tool, the paper introduces a *micromechanical* Taylor factor, which differs from the *macromechanical* Taylor factor by the fact that crystal shear is normalized by the *local* rather than the *global* von Mises strain. © 2001 Acta Materialia Inc. Published by Elsevier Science Ltd. All rights reserved.

**Keywords:** Texture; Theory & modeling — structural behavior; Mechanical properties — plastic; Metals — crystalline; Mesostructure

### 1. INTRODUCTION

#### 1.1. The importance of grain scale heterogeneity in polycrystal plasticity

The anisotropic nature of crystal slip usually entails reorientation and subdivision phenomena during plastic straining of crystalline matter, even under homogeneous and gradient-free external loadings. This leads to spatial heterogeneity in terms of strain, stress, and crystal orientation. The present investigation is concerned with such heterogeneity placing particular attention on grain-to-grain and in-grain phenomena.

Beyond the aim of gaining fundamental insight into polycrystal plasticity, an improved understanding of grain-scale heterogeneity is important for five main practical reasons:

First, structural and functional devices are increasingly miniaturized. This involves size reduction down to the single crystal or crystal-cluster scale. In such parts crystallinity becomes the dominant origin of desired or undesired anisotropy. Tailoring of texture-conditioned quasi-isotropy is no longer possible.

Second, in miniaturized devices plastic heterogeneity and strain localization can be sources of quality loss and failure. Optimized design of small crystalline parts thus requires improved insight into crystal response and kinematics at the grain- and subgrain scale under elastic, plastic, or thermal loadings.

Third, the quantification of elastic–plastic interaction between neighboring grains during straining is relevant for the improvement and verification of polycrystal homogenization models. These are valuable tools for the fast calculation of elastic–plastic anisotropy (e.g. yield locus theory) and deformation texture (e.g. grain interaction Taylor–Bishop–Hill theory) of polycrystalline bulk material.

<sup>†</sup> To whom all correspondence should be addressed. Tel.: +49-211-6792-340/278; fax: +49-211-6792-333  
E-mail address: raabe@mpie.de (D. Raabe)

Fourth, micromechanical test methods such as nano-indentation serve increasingly as tools for the characterization of the elastic–plastic response of samples at scales below the grain size. Consideration of orientation kinematics and kinetics will allow a more detailed analysis of such microscopic force–displacement data. Similar arguments apply in general for mechanical tests where microstructural scales are similar to the sample size.

Fifth, areas with micromechanical stress–strain localization are preferred nucleation sites for homo- and heterophase transformations.

### 1.2. Investigation of grain-scale heterogeneity of plastically strained samples

The application of novel experimental and theoretical methods gradually enriches our knowledge of crystal-scale heterogeneity. Experimental investigations have particularly benefited from new techniques such as the grain-scale determination of displacement fields [1–4] and corresponding microdiffraction methods [5–13].

Theoretical investigations have particularly profited from the introduction of crystal plasticity finite element methods [14–22]. These are employed for two major purposes, namely, for the computation of mechanical response and for the prediction of microstructure evolution. In either case the experimental or model microstructure to be investigated must be mapped onto an appropriate finite element mesh.

The particular strength of crystal plasticity finite element methods lies in the application of realistic boundary conditions to realistic microstructures. This enables the user to take into account both, external loadings and internal crystalline constitutive response at the same time. However, when aiming at investigating genuine constitutive response at the grain-to-grain and in-grain level, a major challenge of heterogeneity research lies in the separation of external (macromechanical) and internal (micromechanical) effects.† Otherwise, it is conceivable that crystal-scale plasticity phenomena are misinterpreted, due to the overlap of macromechanical heterogeneity imposed by geometry and friction conditions on the one hand and micromechanical heterogeneity introduced by grain kinematics, grain interaction, and grain boundaries on the other hand. For instance, when investigating grain interaction phenomena it would be desirable to identify interaction mechanisms independent of friction and sample geometry.

This article presents a novel combination of experimental and theoretical means to address macromechanical and micromechanical effects in grain scale plasticity experimentation and simulation. The main steps are: First, a polycrystalline aluminum sample

with a quasi-2D layer of columnar coarse grains is plastically strained in a channel die experiment. Second, the microtexture is determined by analysis of electron back scattering patterns obtained in a scanning electron microscope before and after straining. Third, the plastic microstrains at the sample surface are calculated from the 3D plastic displacement field determined via photogrammetry. Fourth, the experimental starting data are mapped onto a finite element mesh. Fifth, continuum and crystal plasticity finite element simulations of the channel die experiment are conducted. Sixth, the crystal plasticity simulations are used for separating and analyzing macromechanical and micromechanical effects.

## 2. SAMPLE PREPARATION AND EXPERIMENTAL PROCEDURE

The experiments for the determination of plastic strain and texture heterogeneity comprised the following steps:

First, a coarse grained aluminum sample was cut from a recrystallized polycrystalline sheet containing >99,99 wt.% Al. A quasi 2D layer of grains with columnar morphology was prepared by heating samples into the grain growth and subsequent tertiary recrystallization regime. The final average grain size was 3500  $\mu\text{m}$ . Each sample was polished and etched after the annealing procedure. Considering gradual elongation of the sample during deformation and the limitations given by the chamber of the electron microscope a sample size of 17×10 mm and a thickness of 3 mm was chosen.

Second, crystal orientation maps at the sample surface were determined. Orientation mapping is a technique used to analyze local texture and grain boundary topology in crystalline material. Lattice orientations were measured on a regular grid by automated acquisition and processing of electron backscatter diffraction patterns in the scanning electron microscope using a step size of 100  $\mu\text{m}$ . In order to determine the lattice rotation during plain–strain compression the orientation map was determined before and after deformation.

Third, plane strain compression experiments were conducted using a servo-hydraulic mechanical testing machine equipped with a channel die set-up. Solid-state lubrication was obtained by placing a Teflon foil of 80  $\mu\text{m}$  thickness around the sample. Experiments were carried out at a strain rate of  $1.7\times 10^{-5} \text{ s}^{-1}$  at ambient temperature. Plastic deformation proceeded in a series of subsequent steps each imposing a macroscopic engineering thickness reduction of about 3%. After each step orientation maps and digital images of the sample surface were taken.

Fourth, the 3D plastic displacement field was determined after each straining step using a photogrammetric method. This is a digital image analysis method which is based on the recognition of geometrical changes in the grain scale distribution of sur-

† In this paper the term *micromechanics* refers to microscopic crystal plasticity phenomena at the grain scale.

face patterns before and after straining [23]. Both, the natural characteristics of an unprepared surface or an artificial quasi-stochastic color spray applied to a polished surface may serve as pattern. In order to measure the 3D surface coordinates digital stereo pair images of the sample were acquired using two high resolution CCD cameras. Pattern recognition was carried out by a digital image processing procedure which maps a rectangular grid onto the image. The grid points were characterized by the gray scale distribution around them. After straining the pattern was recognized based on the assumption that the gray scale distribution around a certain coordinate remained unchanged. From the change in border coordinates containing the correct distribution around the grid point the 3D displacement field was calculated. This information served as input for the calculation of the surface components of the local strain tensor using the first order approximation of the standard polar decomposition.

In this study a fine white color spray was applied to the polished surface of the undeformed sample. After recording the pattern the sample was plane strain compressed in a channel die. After each deformation step the surface pattern was acquired and the displacement field as well as the strain distribution were calculated.

### 3. EXPERIMENTAL RESULTS

Figure 1 shows the microtexture of the sample before straining using separate gray scales for the crystallographic axes parallel to the longitudinal direction (RD) and normal direction (ND). The grain structure is revealed by mapping the misorientations among neighboring measuring points. Thin lines indicate orientation changes between  $5^\circ$  and  $15^\circ$ . Fat lines indicate orientation changes above  $15^\circ$ .

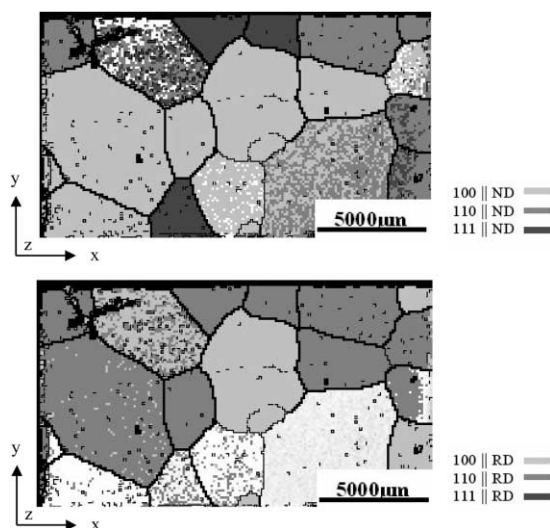


Fig. 1. Microtexture of the sample before straining using separate gray scales for the crystallographic axes parallel to the longitudinal direction (RD) and normal direction (ND). Thin lines indicate orientation changes between  $5^\circ$  and  $15^\circ$ . Fat lines indicate orientation changes above  $15^\circ$ .

cate orientation changes between  $5^\circ$  and  $15^\circ$ . Thick lines indicate orientation changes above  $15^\circ$ .

Figure 2 shows the in-plane distribution of the accumulated plastic von Mises strain in the specimen after 8% sample thickness reduction (the thickness reduction is given by  $\Delta d/d$ , where  $d$  is the sample extension along the compression direction). The strains were calculated from the displacement field which was determined by use of the photogrammetric method explained in the preceding section. The grain boundaries indicated by white lines were taken from the microtexture measurement.

Figure 2 reveals that some grain portions show much higher accumulated plastic strain than others. While some crystals have accumulated as little as 1% von Mises strain within their borders, others show maximum strains beyond 15%, particularly close to some of the grain boundaries. Related to the total macroscopic strain of 8% this gives a large spectrum of  $-87.5\%$  to  $+87.5\%$  deviation from the average value. It is an important observation that such heterogeneity occurs already at a low macroscopic sample strain of only 8%. It can be qualitatively interpreted in terms of the different kinematic hardness (orientation factor) of the grains, although the observed spatial variation in the accumulated plastic strain exceeds the spread expected from the variation in orientation factor under polyslip conditions [24–26]. At larger strains it was found that grain scale strain hardening gradually equilibrates initial hardness differences among the grains, i.e. grain-to-grain strain heterogeneity was less pronounced at larger loadings [4].

It is noteworthy that gradients ranging from 2% to 15% strain occur inside some crystals (e.g. grain 2 in Fig. 2). This effect seems to be promoted by strain localization in front of grain boundaries. In other areas, however, the distribution of strain is not much affected by grain boundaries (e.g. grains 10 and 14 or grains 13 and 14 in Fig. 2). In these areas straining proceeds as a cluster–deformation process, i.e. neighboring crystals co-deform with similar strain on either side of the shared grain boundary. While grains 10 and 14 have a misorientation around  $10^\circ$ , grains 13 and 14 have a misorientation above  $15^\circ$ .

### 4. CRYSTAL PLASTICITY AND CONTINUUM FINITE ELEMENT SIMULATIONS

The microstructure of the undeformed sample was mapped onto an appropriate finite element mesh, Fig. 3. Mesh configuration was conducted along the grain boundaries using a bilinear element with 4 nodes and 4 integration points. The total number of elements was 5705. The finite element calculations were conducted under external plane strain boundary conditions using different friction coefficients. Both simulations (continuum, crystal plasticity) used identical mesh and boundary conditions. The constitutive crystal plasticity description was implemented employing the method of Kalidindi *et al.* [17] using

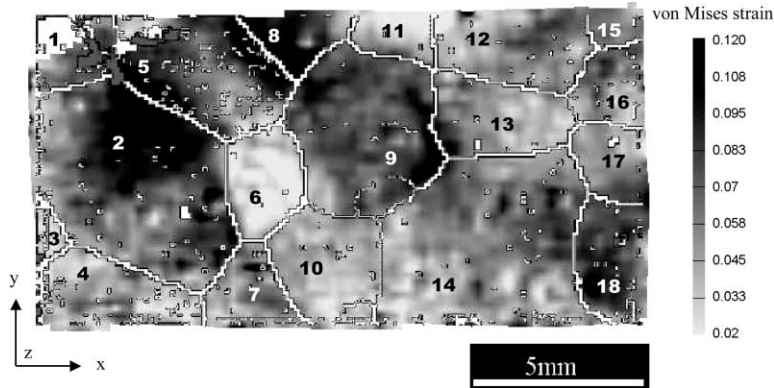


Fig. 2. In-plane distribution of the accumulated plastic von Mises strain in the specimen after 8% sample thickness reduction ( $\Delta d/d$ , where  $d$  is the sample extension along compression direction). The strains were calculated from the displacement field which was determined by use of a photogrammetric method. The grain boundaries indicated by white lines were taken from the microtexture measurement (see Fig. 1).

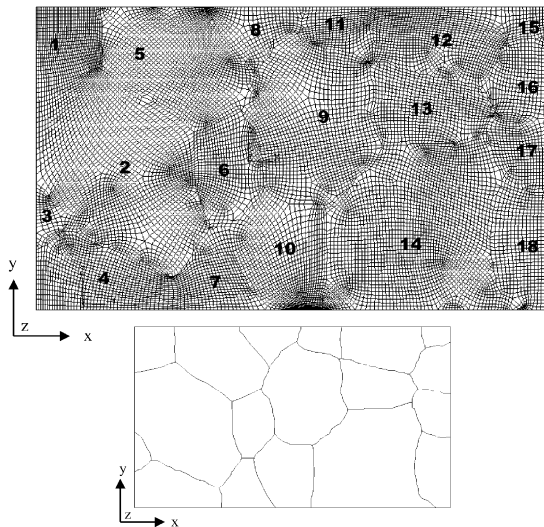


Fig. 3. The microstructure of the undeformed sample was mapped onto a finite element mesh. Mesh configuration was conducted along the grain boundaries using a bilinear element with 4 nodes and 4 integration points. The total number of elements was 5705.

12  $\{111\}\langle 110\rangle$  slip systems and viscoplastic hardening. Calculations were carried out using the finite element program ABAQUS in conjunction with the user defined material subroutine UMAT [27].

Figure 4 shows the continuum and crystal plasticity finite element results for different friction coefficients (8% thickness reduction). The figures show the von Mises strain data back mapped onto the sample shape prior to straining. The continuum solutions show for non-zero friction coefficients localization of the plastic strain along the diagonals with strong maxima at the corners and a less pronounced maximum in the sample center. Minima appear in the middle of the four edges. The crystal plasticity finite element solutions show a much more heterogeneous distribution of strain. In some areas they show strain patterns which reproduce the topology given by the large

angle grain boundaries. Pronounced localization of the plastic strain can be seen along the upper left and lower right part of the shape diagonal as well as within the center grain. Some isolated grains also reveal pronounced strain accumulation. Areas with little plastic strain can be found in the vicinity of the middle of the top and bottom edges. Some grains reveal very small overall strains within their borders. While the continuum predictions reveal a strong dependence of strain heterogeneity on friction (Fig. 4a, c and e), the dependence is less pronounced in the crystal plasticity results (Fig. 4b, d and f). The simulated polycrystal reveals pronounced strain heterogeneity and shear localization not only for friction coefficients of  $\mu = 0.1$  and  $0.2$  but also for  $\mu = 0.01$ .

Very similar results with pronounced strain localization close to the sample diagonals and nonuniform strain distribution in the other areas were also found in earlier crystal plasticity finite element simulations for instance by Dève *et al.* [14] and Harren and Asaro [15]. These authors stated that nonuniform deformation and strain localization naturally arise in polycrystals as a consequence of crystallographic slip. This observation can be fully confirmed by the present crystal plasticity finite element results for near-zero friction conditions (Fig. 4b). However, for cases with non-zero friction coefficients interpretation of the data is less straightforward due to the mixed influence of macro- and microplastic effects on the overall strain profile (Figs 4d, f and 5).

## 5. LIMITATIONS OF THE ANALYSIS

The joint analysis of experimentally determined and simulated microstrains and microtextures gives a qualitative impression of macroscopic, grain-to-grain, in-grain strain heterogeneity. However, *quantitative* analysis of the unprocessed data is limited, due to the overlap of the macromechanical and micromechanical influence on the overall strain profile. It is at this stage not clear, whether the observed nonuniform strain

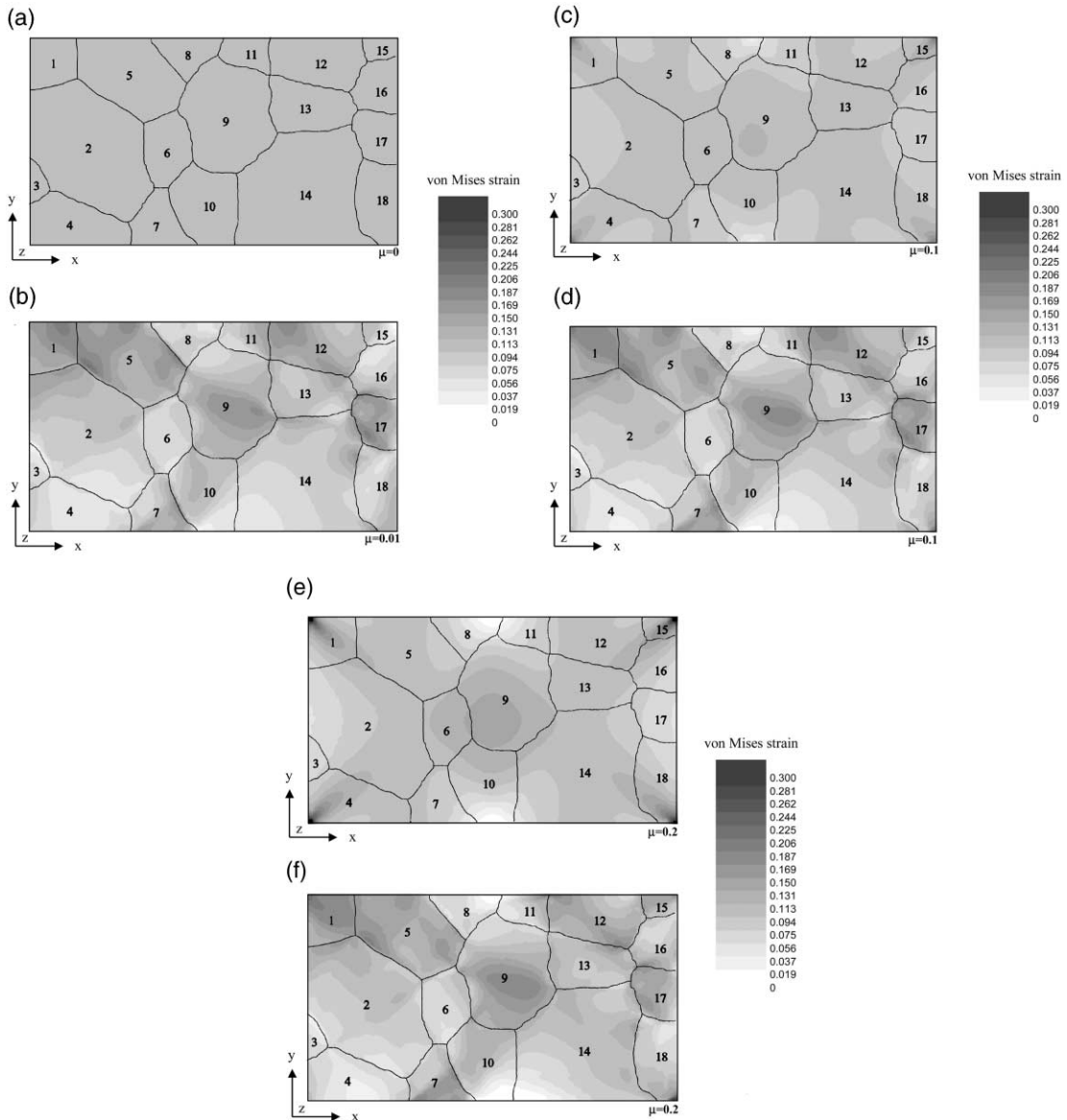


Fig. 4. Continuum and crystal plasticity finite element results for different friction coefficients (8% sample thickness reduction). The figures show the von Mises strain data back mapped onto the sample shape prior to straining. (a) continuum finite element simulation, friction coefficient 0.00; (b) crystal plasticity finite element simulation, friction coefficient 0.01; (c) continuum finite element simulation, friction coefficient 0.1; (d) crystal plasticity finite element simulation, friction coefficient 0.1; (e) continuum finite element simulation, friction coefficient 0.2; (f) crystal plasticity finite element simulation, friction coefficient 0.2.

profiles (experimental: Fig. 2; simulated: Fig. 4f with  $\mu = 0.2$ ) are chiefly due to grain-scale interaction and the presence of grain boundaries or must be attributed to macromechanical effects such as friction and sample geometry. While qualitative comparison of the continuum and crystal plasticity finite element data indicates that the major source of strain heterogeneity is the strong macroscopic strain profile found in both approaches for friction coefficients above zero (Fig. 4c,d and 4e,f), the results for near-zero friction (Fig. 4a and b) reveal a strong *intrinsic* crystallographic tendency for nonuniform straining. These observations are in accord with previous findings obtained

by crystal plasticity finite element simulations which indicated the importance of friction as well as the crystallographic influence on shear localization [14–16, 20–22].

Since this work aims at conducting numerical analysis of experimental data (Fig. 2), particular attention is placed on cases with non-zero friction conditions. This means that quantitative analysis of the crystal plasticity finite element predictions with respect to genuine grain interaction phenomena can only be achieved when heterogeneity effects originated by the macroscopic strain profile are properly taken into account. The following section will address

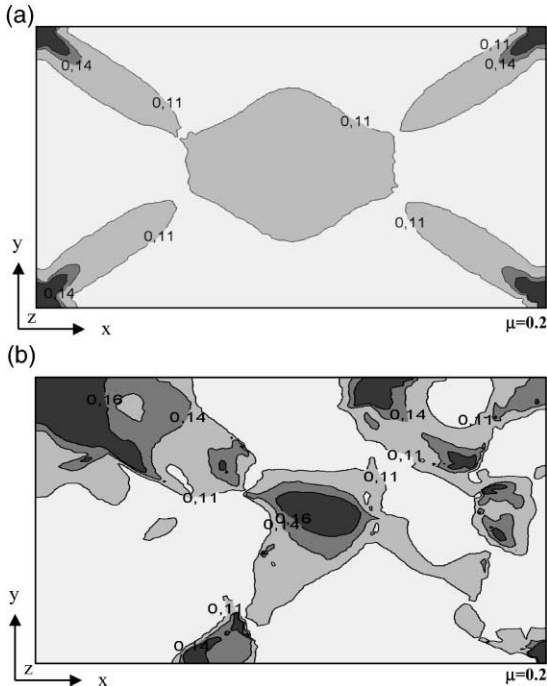


Fig. 5. Macroscopic strain profile (friction coefficient 0.2, 8% sample thickness reduction), data taken from Figs. 4e and f. (a) strain profile in the continuum finite element simulation; (b) strain profile in the crystal plasticity finite element simulation.

these points and introduce measures to analyze crystal plasticity data quantitatively by consideration of the *local* rather than the *global* mechanical loads.

## 6. DISCUSSION OF MACROMECHANICAL AND MICROMECHANICAL EFFECTS

### 6.1. Comparison of continuum and grain scale mechanics

Comparison of the plastic strain fields obtained from continuum and crystal plasticity finite element simulations (Figs 4, 5) reveals three important points:<sup>†</sup> First, the predicted sample shape change is different between the two simulations. Second, the overall strain profile with localization along the diagonals principally appears in both types of simulation. Third, the crystal plasticity simulation predicts a much more heterogeneous distribution of strain and also larger strain gradients than the continuum simulation.

The first observation, i.e. the difference in macroscopic shape change (Fig. 6), is due to the plastic anisotropy of the individual grains in the crystal plasticity approach and the free surface boundary conditions in longitudinal direction.

The second observation, i.e. the localization of

<sup>†</sup> We focus here on simulations with a friction coefficient of 0.2 because they show the best correspondence with the experimental results.

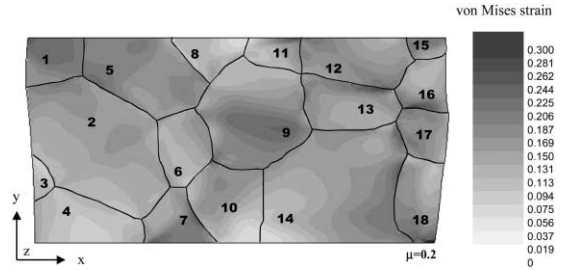


Fig. 6. Crystal plasticity finite element simulation, macroscopic shape change (friction coefficient 0.2, 8% sample thickness reduction).

strain along the diagonals in *both* simulations (non-zero friction), is due to the dominance of friction for the overall strain profile (Fig. 5). However, strain localization appears with different sharpness and symmetry in the two simulations. The continuum prediction shows a symmetric strain profile. The maxima in the corners are much stronger than those in the crystal plasticity simulation (data for  $\mu = 0.2$ , Fig. 4e and f). This indicates the tendency of the crystal plasticity solution to distribute and accommodate external loads in a larger volume than the continuum solution which tends to produce more narrow strain profiles. The crystal plasticity solution reveals a non-symmetric profile of strain (Fig. 5). This can be attributed to the strong kinematic influence of some of the crystals (e.g. grain 6 with high kinematic hardness, i.e. a high Taylor factor). Particularly hard grains seem to modify the overall macroscopic strain path within the specimen.

One approach to identify areas which initiate changes in strain percolation is to subtract the von Mises strain predicted by the continuum simulation from that predicted by the crystal plasticity simulation (Fig. 7). Since both simulations are non-linear and since both, strain and texture evolution are path-dependent, a one-to-one difference map can only give a *topological* impression of the discrepancies between

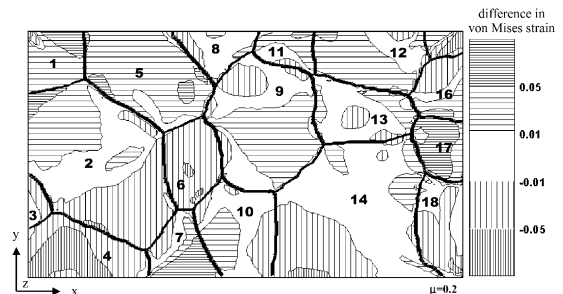


Fig. 7. Subtraction of the von Mises strain predicted by the continuum simulation from that predicted by the crystal plasticity simulation. Since both simulations are non-linear and since both, strain and texture evolution are path-dependent functions, a one-to-one difference map can only give a topological impression of the discrepancies between the two calculations (friction coefficient 0.2, 8% sample thickness reduction).

the two calculations. Figure 7 reveals strong deviations in the corners. Grain 7 shows a pronounced maximum which can be attributed to the above mentioned shift in the diagonal strain path. The same applies for grain 17 which undergoes much stronger deformation in the crystal plasticity simulation than the corresponding areas in the continuum solution. Grains 2, 5, 9, and 12 also show maxima, although less pronounced than grains 1, 5, 7, and 17. Grains 4, 6, 14, and 18 reveal a much smaller von Mises strain than the corresponding areas in the continuum prediction. Particularly grains 4 and 6 have high Taylor factors which might explain the change of the diagonal strain shape, as found in the continuum solution, particularly in this area of the crystal plasticity solution (Fig. 5). This analysis suggests, that through-sample strain percolation follows grains which are kinematically soft and avoids grains which are kinematically hard.

The third observation, i.e. the strong heterogeneity of strain as predicted by the crystal plasticity simulation and observed experimentally, can be attributed to the *joint* influence of macromechanical and micromechanical effects. This means that strain effects at the grain scale result from gradients in the macroscopic strain (friction), the individual kinematic hardness of the crystals (Taylor factors), grain interaction with neighbor crystals, and geometrical grain boundary effects.

The large influence of macromechanics, i.e. of friction on the strain profile is evident from Figs 4a, c, e and 5 which show increasing through-sample strain heterogeneity with increasing friction coefficient for a continuum specimen. The influence of crystallinity on the through-sample profile of strain is indicated by Fig. 4a and b, where friction is practically absent. Figure 4a shows a completely homogeneous macroscopic strain profile for the continuum solution, but the crystal plasticity solution (Fig. 4b) reveals strong heterogeneity of strain (in the crystal plasticity simulation a very small friction coefficient of 0.01 had to be used for reasons of convergence). Furthermore, the importance of grain kinematics is supported by the fact that strain minima and maxima are in the crystal plasticity simulations (and in the experiment, Fig. 2) in some cases well localized within individual grains. This indicates a significant influence of kinematic hardness at least in some portions of the sample. Figure 8 supports this point. It shows a map of the simulated accumulated *local* crystal shear  $\sum \gamma^{\text{local}}$  divided by the *global* (externally exerted) von Mises strain,  $\sum \gamma^{\text{local}} / \langle \epsilon_{\text{VM}} \rangle^{\text{global}}$  (Fig. 8a), and a map of the simulated accumulated *local* crystal shear  $\sum \gamma^{\text{local}}$  divided by the *local* von Mises strain,  $\sum \gamma^{\text{local}} / \langle \epsilon_{\text{VM}} \rangle^{\text{local}}$  (Fig. 8b). The term *local* (local crystal shear, local von Mises strain) means, that these data were counted at each integration point without conducting grain-scale

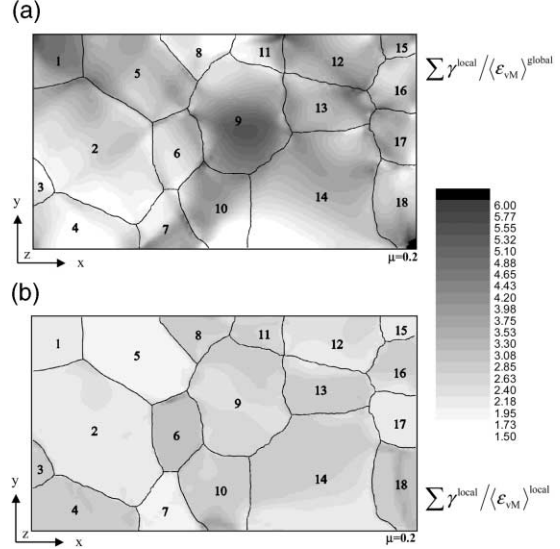


Fig. 8. (a) Map of the simulated accumulated local crystal shear  $\sum \gamma^{\text{local}}$  divided by the global (externally exerted) von Mises strain,  $\sum \gamma^{\text{local}} / \langle \epsilon_{\text{VM}} \rangle^{\text{global}}$ . This quantity is referred to as a macromechanical Taylor factor,  $M^{\text{macro}}$ , because  $\langle \epsilon_{\text{VM}} \rangle^{\text{global}}$  is a constant (the macromechanical Taylor factor is as a rule not identical to the Taylor factor calculated by homogenization theory). (b) Map of the simulated accumulated local crystal shear  $\sum \gamma^{\text{local}}$  divided by the local von Mises strain,  $\sum \gamma^{\text{local}} / \langle \epsilon_{\text{VM}} \rangle^{\text{local}}$ . This quantity is referred to as a micromechanical Taylor factor,  $M^{\text{micro}}$ .

averaging. The latter quantity,  $\sum \gamma^{\text{local}} / \langle \epsilon_{\text{VM}} \rangle^{\text{local}}$ , can be referred to as a *micromechanical Taylor factor*,  $M^{\text{micro}}$ , since it normalizes the local crystallographic shear by the *local* von Mises strain  $\langle \epsilon_{\text{VM}} \rangle^{\text{local}}$  rather than by the *global* (externally exerted) von Mises strain  $\langle \epsilon_{\text{VM}} \rangle^{\text{global}}$ . The shear, as normalized in Fig. 8a,  $\sum \gamma^{\text{local}} / \langle \epsilon_{\text{VM}} \rangle^{\text{global}}$ , can be referred to as a *macromechanical Taylor factor*,  $M^{\text{macro}}$ , because  $\langle \epsilon_{\text{VM}} \rangle^{\text{global}}$  is a constant. It must be noted though that the macromechanical Taylor factor is as a rule *not* identical to the classical Taylor factor calculated by homogenization theory: In the crystal plasticity finite element simulation the local crystal shear  $\sum \gamma^{\text{local}}$  at each integration point follows the *local* and not the *global* boundary conditions, as in classical Taylor–Bishop–Hill-type homogenization theory ( $M^{\text{homog}} = \sum \gamma^{\text{local}} / \langle \epsilon_{\text{VM}} \rangle^{\text{global}}$ ).

The macromechanical Taylor factor (Fig. 8a) reveals a very heterogeneous spatial distribution, similar as the von Mises strain map given in Figs 4–6. After normalization by the correct *local* strain, i.e. by the *total* von Mises strain at each integration point (Fig. 8b), the same shear data show a much more homogeneous distribution within the grains, but still strong grain-to-grain heterogeneity. Different grains with different kinematic hardness (expressed in terms of the micromechanical Taylor factor) appear as rela-

tively homogeneous mechanical entities. This analysis shows that the hardness variations introduced by the texture *modulate* rather than *determine* the strain path prescribed by external conditions such as friction and tensor mode. Large in-grain strain heterogeneity, as observed in Figs 4, 5, 6, and 8a must therefore be mainly attributed to the macroscopic boundary conditions. Owing to Fig. 8b grain interaction and grain boundary phenomena seem to play a smaller role for in-grain strain heterogeneity than first anticipated from Figs 4–6. For instance, grains 1, 2, 5, 7, and 17 reveal a very small and nearly constant micromechanical Taylor factor. In contrast, grains 3, 4, 6, 8, 10, 11, 16, and 18 have high micromechanical Taylor factors, in part with in-grain strain gradients (especially grains 10 and 18).

### 6.2. Separation of grain scale kinematics and grain interaction effects

For a qualitative separation of crystal kinematics and grain interaction/grain boundary effects we compare the experimental data (Fig. 2) with the crystal plasticity simulation using a friction coefficient of 0.2 (Figs 4f and 5b). In the simulation the grain boundaries are simple geometrical obstacles† to plasticity, but dislocation dynamic effects such as dislocation pile ups and geometrically necessary dislocations are not included in the constitutive description. The strain profile predicted by the crystal plasticity finite element simulation reveals in most grains a decent correspondence to the experimental results. For instance grains 4, 5, 6, 13, 14, 15, show very similar strain distribution in their interiors. However, some significant dissimilarities become apparent, too. For example, grain 2 shows in the experiment a much stronger strain gradient towards grain 5 than in the simulation. The situation in grain 9 has the opposite tendency. The simulation predicts a significant strain gradient with minima at the grain boundaries and a pronounced maximum in the center. This resembles the continuum strain profile which has a strain maximum in the intersection of the two diagonals. However, the gradient inside grain 9 in the experiment points at the triple junctions between grains 9, 13, 14, grains 5, 8, 9, and grains 5, 6, 9, respectively. Similar strain localization appears at the triple point between grains 1, 2, 5.

A better separation of in-grain kinematics and grain interaction/grain boundary effects can be achieved by investigating *changes* rather than absolute values of the micromechanical Taylor factor. Figure 9 shows the distribution of the largest component of the gradient of the micromechanical Taylor factor (Fig. 8b). The figure reveals strong plastic effects in the vicinity of most grain boundaries, for instance between grains 5/6, 2/6, and 7/10. Other grain boundaries do not show relevant mechanical effects, e.g. 6/10, 10/14,

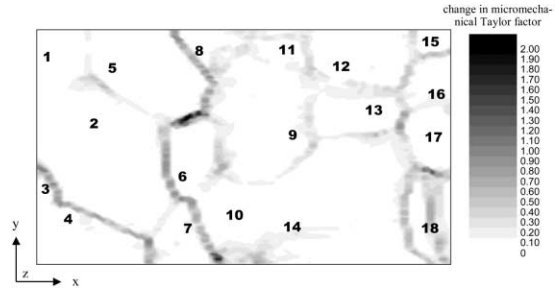


Fig. 9. Distribution of the largest component of the gradient of the micromechanical Taylor factor (Fig. 8b). Strong plastic effects appear in the vicinity of grain boundaries and triple junctions.

and 1/2. As a rule, grain boundary effects are more pronounced at triple points rather than at straight boundary segments. Similar observations were reported by Harren and Asaro [15], who also found in their crystal plasticity calculations stronger effects at triple junctions than along grain boundaries. They stated that triple junctions might even act as sources for the beginning of strain localization. Furthermore, they analyzed simulated strain localization effects as a function of the orientation change across a grain boundary segment. They found that grain boundary effects were less pronounced for small misorientations. Recent work about the *intrinsic* tendency of grains to undergo orientation fragmentation and initiate strain heterogeneity, even under uniform external loads, has revealed, that not only misorientation but also the grain orientation itself plays an important role for strain localization [28].

However, comparison between the texture and the micromechanical Taylor factor in regions with strain localization reveals that the observed gradients are not due to orientation changes but due to grain interaction. Since the overall thickness reduction of the sample investigated is only 8%, the areas affected by plastic grain interactions are relatively small. While the unprocessed data (Fig. 2: experimental; Fig. 4f: simulation) suggest large interaction zones at least for some pairs of grains (e.g. grains 2 and 5), Fig. 9 reveals that these effects can essentially be attributed to the macromechanical influence on the strain profile.

## 7. CONCLUSIONS

We investigated the influence of macromechanical and micromechanical effects in plain-strain polycrystal experimentation and simulation. The main conclusions are:

Plain strain experiments and simulations (continuum FE and crystal plasticity FE with non-zero friction) reveal strain localization along the diagonals with maxima at the corners and a less pronounced maximum in the sample center.

The overall strain profile created in a plastic continuum during plain-strain compression with non-zero

† Change in Schmid factor across a grain boundary.

friction is principally similar to the strain profile found in crystal plasticity simulation and experimentation.

Mechanical analysis of strain heterogeneity is made possible through normalization of the *local* crystallographic shear by the *local* von Mises strain. This quantity is termed *micromechanical Taylor factor*. It must be clearly separated from the macromechanical Taylor factor and from the Taylor factor known from homogenization theory.

The conventional Taylor factor and the macromechanical Taylor are no adequate measures for investigating strain heterogeneity in polycrystals, particularly for non zero friction conditions.

An analysis based on the micromechanical Taylor factor shows that in-grain strain heterogeneity is strongly determined by macroscopic boundary conditions (geometry, friction), but grain interaction effects play a minor role. It reveals further that grain-to-grain strain heterogeneity is strongly affected by crystal kinematics.

Although the continuum solution for the plastic strain reveals similar tendencies as the crystal plasticity solution, the percolation path of strain through the sample is significantly modulated by crystal kinematics. The strain path follows soft crystals and avoids hard crystals.

The investigation shows strain localization at triple points and at most grain boundaries. The grain interaction zones, calculated from the gradients of the micromechanical Taylor factor, are localized in the immediate vicinity of grain boundaries.

#### REFERENCES

1. Delaire, F., Raphanel, J. L. and Rey, C., *Acta mater.*, 2000, **48**, 1075.
2. Nugent, E. E., Calhoun, R. B. and Mortensen, A., *Acta mater.*, 2000, **48**, 1451.
3. Vacher, P., Dumoulin, S., Morestin, F. and Mguil-Touchal, S., *Proc. Inst. Mech. Eng. Part C, J. Mech. Eng. Sci.*, 1999, **213**, 811.
4. Sachtleber, M. and Raabe, D., soon to be published.
5. Weiland, H. and Becker, R. C., in *Proceedings 20. RISØ International Symposium on Materials Science*, ed. T. Lefers and O. P. Pederson. RISØ National Laboratory, Roskilde, Denmark, 1999, p. 213.
6. Weiland, H. and Schwarzer, R. A., in *Proceedings 7th International Conference on Textures of Materials*. Holland, North-Holland, 1984, p. 857.
7. Ørsund, R., Hjelen, J. and Nes, E., *Scripta metall.*, 1989, **23**, 1193.
8. Adams, B. L., Wright, S. I. and Kunze, K., *Metall. Trans.*, 1993, **A24**, 819.
9. Adams, B. L. and Weiland, H. (eds), *Microscale Textures of Materials*, special issue of Textures and Microstructures, 1993, **20**.
10. Zaeferrer, S. and Schwarzer, R. A., *Zeitschrift fuer Metallkunde*, 1994, **85**, 585.
11. Schwarzer, R. A. and Bunge, J. H., *Adv. Eng. Mater.*, 2001, **3**, 25.
12. Hughes, D. A., in *Proceedings 16th International RISØ Symposium on Materials Science*. Roskilde, Denmark, 1995, p. 63.
13. Hughes, D. A. and Kumar, A., in *Proceedings of the 11th International Conference on Textures of Materials ICOTOM 11, 1996, Xi'an, China*, ed. Z. Liang, L. Zuo and Y. Chu. International Academic Publishers, 137 Chaonei Dajie, Beijing 100010, China, 1996, p. 1345.
14. Dève, H., Harren, S. V., McCullough, C. and Asaro, R. J., *Acta metall.*, 1988, **36**, 341.
15. Harren, S. V. and Asaro, R. J., *J. Mech. Phys. Solids*, 1989, **37**, 191.
16. Becker, R. C., *Acta metall.*, 1991, **39**, 1211.
17. Kalidindi, S. R., Bronkhorst, C. A. and Anand, L., *J. Mech. Phys. Solids*, 1992, **40**, 537.
18. Dawson, P. R., Beaudoin, A. J. and Mathur, K. K., in *Proceedings 15. RISØ International Symposium on Materials Science*, ed. S. I. Andersen, J. B. Bilde-Sørensen, T. Lorentzen, O. B. Pedersen and N. J. Sørensen. RISØ National Laboratory, Roskilde, Denmark, 1994, p. 33.
19. Beaudoin, A. J., Mecking, H. and Kocks, U. F., *Phil. mag. A*, 1996, **73**, 1503.
20. Becker, R. C. and Panchanadeeswaran, S., *Acta metall.*, 1995, **43**, 2701.
21. Mathur, K. K. and Dawson, P. R., *Int. J. Plast.*, 1998, **8**, 67.
22. Dawson, P. R., *Int. J. Solids Struct.*, 2000, **37**, 115.
23. Handbook for the Aramis system by GOM mbh, Gesellschaft für Optische Meßtechnik. Version September 2000, Braunschweig, Germany
24. Kocks, U. F., *Acta metall.*, 1958, **6**, 85.
25. Kocks, U. F., *Acta metall.*, 1960, **8**, 345.
26. Hosford, W. F., *The Mechanics of Crystals and Textured Polycrystals*. Oxford University Press, 1993.
27. ABAQUS/Standard User's Manual, Vol. II, 14.1.4-1. Hibbitt, Karlsson and Sorensen, Pawtucket, RI, 1999.
28. Raabe, D., Zhao, Z., Park, S. -J. and Roters, F., (in press).